**48th AIAA Aerospace Sciences Meeting Including the New Horizons Forum and Aerospace Exposition**
**4 - 7 January 2010, Orlando, Florida**

**AIAA 2010-363**

# A Hybridizable Discontinuous Galerkin Method for the Compressible Euler and Navier-Stokes Equations

J. Peraire[*] and N. C. Nguyen[†]

*Massachusetts Institute of Technology, Cambridge, MA 02139, USA*

B. Cockburn[‡]

*University of Minnesota, Minneapolis, MN 55455, USA*

In this paper, we present a Hybridizable Discontinuous Galerkin (HDG) method for the solution of the compressible Euler and Navier-Stokes equations. The method is devised by using the discontinuous Galerkin approximation with a special choice of the numerical fluxes and weakly imposing the continuity of the normal component of the numerical fluxes across the element interfaces. This allows the approximate conserved variables defining the discontinuous Galerkin solution to be locally condensed, thereby resulting in a reduced system which involves only the degrees of freedom of the approximate traces of the solution. The HDG method inherits the geometric flexibility and arbitrary high order accuracy of Discontinuous Galerkin methods, and offers a significant reduction in the computational cost as well as improved accuracy and convergence properties. In particular, we show that HDG produces optimal converges rates for both the conserved quantities as well as the viscous stresses and the heat fluxes. We present some numerical results to demonstrate the accuracy and convergence properties of the method.

## I.   Introduction

The numerical simulation of compressible flows has become an indispensable tool for many important applications such as aero-acoustics, vehicle design and turbomachinery. Although the ever increasing computer power allows us to solve complex problems that would have been intractable a few years ago, there are still many problems of practical interest for which the existing methods are inadequate. Therefore, the development of robust, accurate, and efficient methods for the numerical solution of the compressible Navier-Stokes equations in complex geometries remains a topic of considerable importance. In recent years, discontinuous Galerkin (DG) finite element methods have emerged as a competitive alternative for solving nonlinear hyperbolic systems of conservation laws. The advantages of the DG methods over classical finite difference and finite volume methods are well-documented in the literature:[5,6] the DG methods work well on arbitrary meshes, result in stable high order discretizations of the convective and diffusive operators, allow for a simple and unambiguous imposition of boundary conditions and are very flexible to parallelization and adaptivity. Despite all these advantages, DG methods have not yet made a significant impact for practical applications. This is largely due to the high computational cost associated to DG methods when compared to finite volume schemes.

In this paper, building on the previous work[7–9,13–17] we develop a new class of hybridizable discontinuous Galerkin (HDG) methods for the numerical solution of the compressible Euler and Navier-Stokes equations. In addition to possessing local conservativity, high-order accuracy, and strong stability for convection-dominated flows, the proposed HDG methods have the following main advantages over many existing DG methods. First, unlike many other DG methods (analyzed in Ref. [2]) which result in a final system involving the degrees of freedom of the approximate field variables, the HDG methods produces a final system in terms

---

[*]Professor, Department of Aeronautics and Astronautics, M.I.T., 77 Massachusetts Avenue, AIAA Associate Fellow.
[†]Research Scientist, Department of Aeronautics and Astronautics, M.I.T., 77 Massachusetts Avenue, AIAA Member.
[‡]Professor, School of Mathematics, University of Minnesota, Minneapolis.

of the degrees of freedom of the *approximate traces* of the field variables. Since the approximate traces are defined on the element faces only and single-valued on every face, the HDG methods have significantly less the globally coupled unknowns than other DG methods. This large reduction in the degrees of freedom can lead to significant savings for both computational time and memory storage. Second, the HDG method exhibits optimal convergence properties for the primal variables as well as their fluxes. In fact, to our knowledge, it is the only DG method that achieves optimal convergence of the viscous fluxes in multidimensions. For the compressible Navier-Stokes equations, we show results that indicate that the conserved quantities as well as the viscous stresses and heat fluxes, converge with the optimal convergence of $k + 1$ in the $L^2$- norm, when polynomial approximations of order $k$ are used. Finally, the HDG methods can deal with inflow, outflow, slip, and solid wall boundary conditions weakly in a unified framework by defining appropriate numerical fluxes on the domain boundaries.

The HDG methods are devised by using the discontinuous Galerkin methodology to discretize the compressible Navier-Stokes equations with appropriate choices of the numerical fluxes and by applying the hybridization technique to the resulting discretization. We first introduce the approximate traces of the conserved variables as new unknowns defined on the element boundaries. We then define a total numerical flux (including both the viscous and inviscid terms) in terms of the approximate traces and weakly impose the continuity of the normal component of the numerical flux. This results in a large nonlinear system of equations for the approximate field variables (including velocity, density, and energy and their spatial derivatives) an the trace of the conserved variables. This nonlinear system is solved by using the Newton method. After linearization, we can locally condense all the approximate field variables and their spatial derivatives in an *element-by-element* fashion and obtain a reduced global system involving only the approximate traces of the conserved variables.

Since the first DG method[22] was introduced in 1973 by Reed and Hill for the transport equation, significant developments have been made in the area of discontinuous Galerkin methods[11] for the numerical solution of nonlinear hyperbolic conservation laws. The first DG method[3] for the compressible Navier-Stokes equations were proposed in 1997 by Bassi and Rebay. Shortly after, the local DG method[10] and the Baumann-Oden DG method[4] were developed for convection-diffusion problems. Based upon the work of Basi-Rebay[3] and Cockburn and Shu,[10] Lomtev and Karniadakis also developed a DG method for the Navier-Stokes equations.[12] The compact discontinuous Galerkin method introduced in Ref. [19] has also been applied to compressible viscous flows[20] and turbulent flows.[18] Recently, an interior penalty DG method[21] was proposed by Hartmann and Houston for numerically solving the compressible Navier-Stokes equations. For these DG methods, the use of explicit time-stepping methods proves very attractive since the resulting mass matrix is block-diagonal. However, when an implicit time-stepping method is used, these DG methods produce a discrete system involving a large number of coupled degrees of freedom due to the nodal duplications along the interelement boundaries. Fortunately, this major drawback of many DG methods is not present in the HDG method since its globally coupled unknowns are defined on the element boundaries and are single-valued there.

The paper is organized as follows. We introduce the HDG method for the compressible Euler equations in Section 2 and in the compressible Navier-Stokes equations in Section 3. In each section, we formulate the method, briefly describe its implementation, and discuss the choice of the stabilization matrix and the treatment of the boundary conditions. In Section 4 we provide numerical results to assess the performance of the method. Finally, in Section 5 we present some concluding remarks.

## II.   HDG Method for the Euler Equations

### A.   Governing Equations and Notation

We consider the steady-state Euler equations of gas dynamics defined over a domain $\Omega \subset \mathcal{R}^d$ written in nondimensional conservation form as

$$\nabla \cdot \boldsymbol{F}(\boldsymbol{u}) \quad = \quad 0, \qquad \text{in } \Omega, \tag{1}$$

where $\boldsymbol{u}$ is the $m$-dimensional vector of conserved dimensionless quantities (namely, density, momentum and energy) and $\boldsymbol{F}(\boldsymbol{u})$ are the inviscid fluxes of dimension $m \times d$. The Euler equations (1) must be supplemented with appropriate boundary conditions at the inflow and outflow boundaries and at the solid wall. We discuss these boundary conditions below.

American Institute of Aeronautics and Astronautics

To describe the HDG method for solving the Euler equations, we introduce some notation. We denote by $\mathcal{T}_h$ a collection of disjoint regular elements $K$ that partition $\Omega$ and set $\partial \mathcal{T}_h := \{\partial K : K \in \mathcal{T}_h\}$. For an element $K$ of the collection $\mathcal{T}_h$, $F = \partial K \cap \partial \Omega$ is the boundary face if the $d-1$ measure of $F$ is nonzero. For two elements $K^+$ and $K^-$ of the collection $\mathcal{T}_h$, $F = \partial K^+ \cap \partial K^-$ is the interior face between $K^+$ and $K^-$ if the $d-1$ measure of $F$ is nonzero. We denote by $\mathcal{E}_h^o$ and $\mathcal{E}_h^\partial$ the set of interior and boundary faces, respectively. We set $\mathcal{E}_h = \mathcal{E}_h^o \cup \mathcal{E}_h^\partial$.

Let $\mathcal{P}^k(D)$ denote the space of polynomials of degree at most $k$ on a domain $D$ and let $L^2(D)$ be the space of square integrable functions on $D$. We introduce the following discontinuous finite element approximation space

$$\boldsymbol{W}_h^k = \{\boldsymbol{w} \in (L^2(\mathcal{T}_h))^m : \boldsymbol{w}|_K \in (\mathcal{P}^k(K))^m, \ \forall K \in \mathcal{T}_h\}.$$

In addition, we introduce a finite element approximation space for the approximate trace of the solution

$$\boldsymbol{M}_h^k = \{\boldsymbol{\mu} \in (L^2(\mathcal{E}_h)^m : \boldsymbol{\mu}|_F \in (\mathcal{P}^k(F))^m, \ \forall F \in \mathcal{E}_h\}.$$

Note that $\boldsymbol{M}_h$ consists of functions which are continuous inside the faces (or edges) $F \in \mathcal{E}_h$ and discontinuous at their borders.

Finally, we define various inner products for our finite element spaces. We write $(w,v)_{\mathcal{T}_h} := \sum_{K \in \mathcal{T}_h}(w,v)_K$, where $(w,v)_D$ denotes the integral of $w\,v$ over the domain $D \subset \mathbb{R}^d$ for $w,v \in P_h$. We also write $(\boldsymbol{w},\boldsymbol{v})_{\mathcal{T}_h} := \sum_{i=1}^m (w_i,v_i)_{\mathcal{T}_h}$ for $\boldsymbol{w},\boldsymbol{v} \in \boldsymbol{W}_h^k$. We then write $\langle \eta,\zeta\rangle_{\partial \mathcal{T}_h} := \sum_{K \in \mathcal{T}_h}\langle \eta,\zeta\rangle_{\partial K}$ and $\langle \boldsymbol{\eta},\boldsymbol{\zeta}\rangle_{\partial \mathcal{T}_h} := \sum_{i=1}^m \langle \eta_i,\zeta_i\rangle_{\partial \mathcal{T}_h}$, for $\boldsymbol{\eta},\boldsymbol{\zeta} \in \boldsymbol{M}_h^k$, where $\langle \eta,\zeta\rangle_D$ denotes the integral of $\eta\,\zeta$ over the domain $D \subset \mathbb{R}^{d-1}$.

## B.    Formulation of the HDG Method

We seek an approximation $\boldsymbol{u}_h \in \boldsymbol{W}_h^k$ such that for all $K \in \mathcal{T}_h$,

$$-(\boldsymbol{F}(\boldsymbol{u}_h), \nabla \boldsymbol{w})_K + \left\langle \widehat{\boldsymbol{F}}_h \cdot \boldsymbol{n}, \boldsymbol{w} \right\rangle_{\partial K} = 0, \quad \forall \boldsymbol{w} \in (\mathcal{P}^k(K))^m. \tag{2}$$

Here, the numerical flux $\widehat{\boldsymbol{F}}_h$ is an approximation to $\boldsymbol{F}(\boldsymbol{u})$ over $\partial K$. We take the numerical flux of the form

$$\widehat{\boldsymbol{F}}_h \cdot \boldsymbol{n} = \boldsymbol{F}(\widehat{\boldsymbol{u}}_h) \cdot \boldsymbol{n} + \boldsymbol{S}(\boldsymbol{u}_h, \widehat{\boldsymbol{u}}_h)(\boldsymbol{u}_h - \widehat{\boldsymbol{u}}_h), \quad \text{on } \partial K, \tag{3}$$

where $\widehat{\boldsymbol{u}}_h \in \boldsymbol{M}_h^k$ is an approximation to the trace of the solution $\boldsymbol{u}$ on $\partial K$, and $\boldsymbol{S}(\boldsymbol{u}_h, \widehat{\boldsymbol{u}}_h)$ is a *local stabilization matrix* which has an important effect on both the stability and accuracy of the resulting scheme. Alternative definitions for the numerical flux are given in Ref. [14]. The selection of the matrix $\boldsymbol{S}$ will be described below.

By adding the contributions of (2) over all the elements and enforcing the continuity of the normal component of the numerical flux, we arrive at the following problem: find an approximation $(\boldsymbol{u}_h, \widehat{\boldsymbol{u}}_h) \in \boldsymbol{W}_h^k \times \boldsymbol{M}_h^k$ such that

$$\begin{aligned}
-(\boldsymbol{F}(\boldsymbol{u}_h), \nabla \boldsymbol{w})_{\mathcal{T}_h} + \left\langle \widehat{\boldsymbol{F}}_h \cdot \boldsymbol{n}, \boldsymbol{w} \right\rangle_{\partial \mathcal{T}_h} &= 0, \qquad \forall \boldsymbol{w} \in \boldsymbol{W}_h^k, \\
\left\langle \widehat{\boldsymbol{F}}_h \cdot \boldsymbol{n}, \boldsymbol{\mu} \right\rangle_{\partial \mathcal{T}_h \setminus \partial \Omega} + \left\langle \widehat{\boldsymbol{B}}_h, \boldsymbol{\mu} \right\rangle_{\partial \Omega} &= 0, \qquad \forall \boldsymbol{\mu} \in \boldsymbol{M}_h^k.
\end{aligned} \tag{4}$$

Here $\widehat{\boldsymbol{B}}_h$ is the numerical flux vector of dimension $m$ and is defined over the boundary $\partial \Omega$. Its precise definition depends on the types of boundary conditions and will be given below. Note that $\widehat{\boldsymbol{u}}_h$ is single-valued over each edge since $\widehat{\boldsymbol{u}}_h$ belongs to $\boldsymbol{M}_h^k$. Furthermore, we note that even though the quantity $[\![\widehat{\boldsymbol{F}}_h \cdot \boldsymbol{n}]\!]$ may not be zero pointwise, its projection is, that is, $\mathsf{P}[\![\widehat{\boldsymbol{F}}_h \cdot \boldsymbol{n}]\!] = 0$, where $\mathsf{P}$ denotes the $L^2$ projection into $\boldsymbol{M}_h^k$. Therefore, our scheme is conservative since only the projection of $\widehat{\boldsymbol{F}}_h \cdot \boldsymbol{n}$ enters the first equation in (4).

By applying the Newton-Raphson procedure to solve the weak formulation (4) we obtain at every Newton step a matrix system of the form

$$\begin{bmatrix} A & B \\ C & D \end{bmatrix} \begin{pmatrix} U \\ \Lambda \end{pmatrix} = \begin{pmatrix} F \\ G \end{pmatrix},$$

where $U$ and $\Lambda$ are the vectors of degrees of freedom of $\boldsymbol{u}_h$ and $\widehat{\boldsymbol{u}}_h$, respectively. It is important to note that the matrix $A$ has block-diagonal structure. Therefore, we can eliminate $U$ to obtain a reduced system in terms of $\Lambda$ as

$$\mathbb{K}\,\Lambda = \mathbb{R},$$

American Institute of Aeronautics and Astronautics

where $\mathbb{K} = D - CA^{-1}B$ and $\mathbb{R} = G - CA^{-1}F$. This is the global system to be solved at every Newton iteration. Since $\widehat{\boldsymbol{u}}_h$ is defined and single-valued along the faces, the final matrix system of the HDG method is smaller than that of many other DG methods. Moreover, the matrix $\mathbb{K}$ is compact in the sense that only the degrees of freedom between neighboring the faces that share the same element are connected.

## C. Stabilization Matrix

We propose here two schemes to define the stabilization matrix. In the first scheme, we choose

$$\boldsymbol{S} = \boldsymbol{L}|\boldsymbol{\Lambda}|\boldsymbol{R}, \tag{5}$$

where $\boldsymbol{L}$, $\boldsymbol{R}$, and $\boldsymbol{\Lambda}$ are the matrices of the left and right eigenvectors, and eigenvalues of the Jacobian matrix $[\partial \boldsymbol{F}(\widehat{\boldsymbol{u}}_h)/\partial \widehat{\boldsymbol{u}}_h] \cdot \boldsymbol{n}$, respectively. The second scheme inspired by the local Lax-Friedrich method involves choosing

$$\boldsymbol{S} = \lambda_{\max}\boldsymbol{I}, \tag{6}$$

where $\lambda_{\max}$ is the maximum absolute value of the eigenvalues of the matrix $\boldsymbol{\Lambda}$, and $\boldsymbol{I}$ is the identity matrix.

The proposed schemes appear to be new as the stabilization matrix depends only on one state defined over the element interface. In contrast, traditional finite volume and DG methods define the stabilization matrix as a function of two states defined over two opposite sides of the element interface.

## D. Numerical Fluxes

In order to gain some insight into the form of the numerical fluxes and to be able to compare the numerical fluxes used here with the more standard forms used by other DG methods, we insert the expression (3) into the second equation in (4). If we assume just for the purpose of illustration, that the stabilization matrix is constant over a face then we obtain the following expressions for $\widehat{\boldsymbol{u}}_h$ and $\widehat{\boldsymbol{F}}_h \cdot \boldsymbol{n}$,

$$
\begin{aligned}
\widehat{\boldsymbol{u}}_h &= \frac{1}{2}(\boldsymbol{u}_h^L + \boldsymbol{u}_h^R), \\
\widehat{\boldsymbol{F}}_h \cdot \boldsymbol{n}^L &= \boldsymbol{F}(\widehat{\boldsymbol{u}}_h) \cdot \boldsymbol{n}^L + \frac{1}{2}\boldsymbol{S}(\boldsymbol{u}_h^R - \boldsymbol{u}_h^L).
\end{aligned} \tag{7}
$$

Here, $\boldsymbol{u}_h^L$ and $\boldsymbol{u}_h^R$ denote the left and right DG approximations at either side of the interface and $\boldsymbol{n}^L$ is the unit normal to the interface pointing from left side to the right side. We observe that when the stabilization matrix is chosen according to expression (6), then this scheme reduced precisely to the local Lax-Friedrichs scheme. When the stabilization matrix is chosen according to (5), then the resulting scheme resembles Roe's scheme but with some differences.

## E. Boundary Conditions

### 1. Inflow/Outflow boundary conditions

At the inlet section or outlet section of the flow, we need to set the state variable $\boldsymbol{u}$ to the freestream condition $\boldsymbol{u}_\infty$. To this end, we define the boundary flux vector $\widehat{\boldsymbol{B}}_h$ as

$$\widehat{\boldsymbol{B}}_h = \boldsymbol{A}_n^+(\widehat{\boldsymbol{u}}_h)(\boldsymbol{u}_h - \widehat{\boldsymbol{u}}_h) - \boldsymbol{A}_n^-(\widehat{\boldsymbol{u}}_h)(\boldsymbol{u}_\infty - \widehat{\boldsymbol{u}}_h), \tag{8}$$

where $\boldsymbol{A}_n = \boldsymbol{A} \cdot \boldsymbol{n}$ and $\boldsymbol{A}_n^\pm = (\boldsymbol{A}_n \pm |\boldsymbol{A}_n|)/2$. Here $\boldsymbol{A}_n = [\partial \boldsymbol{F}/\partial \boldsymbol{u}] \cdot \boldsymbol{n}$ denotes the Jacobian of the inviscid normal flux to the boundary.

### 2. Slip boundary condition

At the solid surface with slip condition, we must impose zero normal velocity. Henceforth, we set

$$\widehat{\boldsymbol{B}}_h = (\boldsymbol{b}_h - \widehat{\boldsymbol{u}}_h), \tag{9}$$

where the vector $\boldsymbol{b}_h$ is defined in terms of $\boldsymbol{u}_h$ as follows

$$\boldsymbol{b}_h[1] = \boldsymbol{u}_h[1], \quad \boldsymbol{b}_h[2, \ldots, m-1] = \boldsymbol{v}_h - \boldsymbol{n}v_n, \quad \boldsymbol{b}_h[m] = \boldsymbol{u}_h[m]. \tag{10}$$

Here $\boldsymbol{v}_h = \boldsymbol{u}_h[2, \ldots, m-1]$ are the velocity components of $\boldsymbol{u}_h$ and $v_n = \boldsymbol{v}_h \cdot \boldsymbol{n}$ is the normal component of the approximate velocity. Note that since $(\boldsymbol{v}_h - \boldsymbol{n}v_n) \cdot \boldsymbol{n} = 0$ we have $\widehat{\boldsymbol{v}}_h \cdot \boldsymbol{n} = 0$, where $\widehat{\boldsymbol{v}}_h = \widehat{\boldsymbol{u}}_h[2, \ldots, m-1]$ are the velocity components of $\widehat{\boldsymbol{u}}_h$.

American Institute of Aeronautics and Astronautics

**F.   Extension to the Unsteady Euler Equations**

We end this section by extending the HDG method to the unsteady Euler equations

$$\frac{\partial \boldsymbol{u}}{\partial t} + \nabla \cdot \boldsymbol{F}(\boldsymbol{u}) = 0, \qquad \text{in } \Omega \times (0, t_f],$$
$$\boldsymbol{u} = \boldsymbol{u}_0, \qquad \text{on } \Omega \times \{t = 0\}.$$

The boundary conditions are the same as the steady-sate case.

Using the Backward-Euler scheme at time level $t^j$ with timestep $\Delta t^j$ we find an approximation $(\boldsymbol{u}_h^j, \widehat{\boldsymbol{u}}_h^j) \in \boldsymbol{W}_h^k \times \boldsymbol{M}_h^k$ such that

$$\left(\frac{\boldsymbol{u}_h^j}{\Delta t}, \boldsymbol{w}\right) - \left(\boldsymbol{F}(\boldsymbol{u}_h^j), \nabla \boldsymbol{w}\right)_{\mathcal{T}_h} + \left\langle \widehat{\boldsymbol{F}}_h^j \cdot \boldsymbol{n}, \boldsymbol{w} \right\rangle_{\partial \mathcal{T}_h} = \left(\frac{\boldsymbol{u}_h^{j-1}}{\Delta t}, \boldsymbol{w}\right), \qquad \forall \boldsymbol{w} \in \boldsymbol{W}_h^k,$$
$$\left\langle \widehat{\boldsymbol{F}}_h^j \cdot \boldsymbol{n}, \boldsymbol{\mu} \right\rangle_{\partial \mathcal{T}_h \backslash \partial \Omega} + \left\langle \widehat{\boldsymbol{B}}_h^j, \boldsymbol{\mu} \right\rangle_{\partial \Omega} = 0, \qquad\qquad \forall \boldsymbol{\mu} \in \boldsymbol{M}_h^k, \tag{11}$$

where

$$\widehat{\boldsymbol{F}}_h^j \cdot \boldsymbol{n} = \boldsymbol{F}(\widehat{\boldsymbol{u}}_h^j) \cdot \boldsymbol{n} + \boldsymbol{S}(\boldsymbol{u}_h^j, \widehat{\boldsymbol{u}}_h^j)(\boldsymbol{u}_h^j - \widehat{\boldsymbol{u}}_h^j), \tag{12}$$

and the boundary numerical flux $\widehat{\boldsymbol{B}}_h^j$ is already described earlier. This discrete system is similar to the system (4) for the steady-state case except that there are two additional terms due to the backward difference discretization of the time derivative. We can thus apply the same solution procedure described above for the steady-state case to the time-dependent case at every time level.

Since using higher-order BDF schemes or diagonally implicit Runge-Kutta (DIRK) methods would yield a discrete system similar to (11), the HDG method for spatial discretization can also be used with these implicit high-order time-stepping schemes. This leads to a high-order accurate method in both space and time.

# III.   HDG Method for the Navier-Stokes Equations

**A.   Governing Equations**

We consider the steady-state compressible Navier-Stokes equations written in conservation form as

$$\boldsymbol{q} - \nabla \boldsymbol{u} = 0, \qquad \text{in } \Omega,$$
$$\nabla \cdot (\boldsymbol{F}(\boldsymbol{u}) + \boldsymbol{G}(\boldsymbol{u}, \boldsymbol{q})) = 0, \qquad \text{in } \Omega, \tag{13}$$

where $\boldsymbol{G}(\boldsymbol{u}, \boldsymbol{q})$ are the viscous fluxes of dimension $m \times d$. The nondimensional form of the Navier-Stokes equations as well as the definition of the inviscid and viscous fluxes can be found in Ref. [1]. Of course, the Navier-Stokes equations (13) should be supplemented with appropriate boundary conditions at the inflow, outflow and solid wall boundaries, as well as a source term which is omitted for simplicity of exposition. We discuss below how to deal with these boundary conditions.

In addition to the notation introduced in Section II, we need to define a new approximation space as

$$\boldsymbol{V}_h^k = \{\boldsymbol{v} \in (L^2(\mathcal{T}_h))^{m \times d} \ : \ \boldsymbol{v}|_K \in (\mathcal{P}^k(K))^{m \times d}, \ \forall \, K \in \mathcal{T}_h\}.$$

The approximate gradient $\boldsymbol{q}_h$, which approximates $\boldsymbol{q}$, resides in this space.

**B.   Formulation**

Following the method of line for the Euler equations we seek an approximation $(\boldsymbol{q}_h, \boldsymbol{u}_h, \widehat{\boldsymbol{u}}_h) \in \boldsymbol{V}_h^k \times \boldsymbol{W}_h^k \times \boldsymbol{M}_h^k$ such that

$$(\boldsymbol{q}_h, \boldsymbol{v})_{\mathcal{T}_h} + (\boldsymbol{u}_h, \nabla \cdot \boldsymbol{v})_{\mathcal{T}_h} - \langle \widehat{\boldsymbol{u}}_h, \boldsymbol{v} \cdot \boldsymbol{n} \rangle_{\partial \mathcal{T}_h} = 0, \qquad \forall \boldsymbol{v} \in \boldsymbol{V}_h^k,$$
$$-(\boldsymbol{F}(\boldsymbol{u}_h) + \boldsymbol{G}(\boldsymbol{u}_h, \boldsymbol{q}_h), \nabla \boldsymbol{w})_{\mathcal{T}_h} + \left\langle (\widehat{\boldsymbol{F}}_h + \widehat{\boldsymbol{G}}_h) \cdot \boldsymbol{n}, \boldsymbol{w} \right\rangle_{\partial \mathcal{T}_h} = 0, \qquad \forall \boldsymbol{w} \in \boldsymbol{W}_h^k,$$
$$\left\langle (\widehat{\boldsymbol{F}}_h + \widehat{\boldsymbol{G}}_h) \cdot \boldsymbol{n}, \boldsymbol{\mu} \right\rangle_{\partial \mathcal{T}_h \backslash \partial \Omega} + \left\langle \widehat{\boldsymbol{B}}_h, \boldsymbol{\mu} \right\rangle_{\partial \Omega} = 0, \qquad \forall \boldsymbol{\mu} \in \boldsymbol{M}_h^k. \tag{14}$$

American Institute of Aeronautics and Astronautics

Here, the numerical fluxes $\widehat{\boldsymbol{F}}_h$ and $\widehat{\boldsymbol{G}}_h$ are an approximation to $\boldsymbol{F}(\boldsymbol{u})$ and $\boldsymbol{G}(\boldsymbol{u}, \boldsymbol{q})$ over $\partial K$, respectively. In addition, $\widehat{\boldsymbol{B}}_h$ is the numerical flux vector of dimension $m$ defined over the boundary.

As before, we take the interior numerical fluxes of form

$$(\widehat{\boldsymbol{F}}_h + \widehat{\boldsymbol{G}}_h) \cdot \boldsymbol{n} = (\boldsymbol{F}(\widehat{\boldsymbol{u}}_h) + \boldsymbol{G}(\widehat{\boldsymbol{u}}_h, \boldsymbol{q}_h)) \cdot \boldsymbol{n} + \boldsymbol{S}(\boldsymbol{u}_h, \widehat{\boldsymbol{u}}_h)(\boldsymbol{u}_h - \widehat{\boldsymbol{u}}_h), \tag{15}$$

where the stabilization matrix $\boldsymbol{S}$ can be selected by extending the expressions proposed above for the Euler equations. The boundary flux vector $\widehat{\boldsymbol{B}}_h$ depends on the types of boundary conditions, the precise definition of which will be described below.

By applying the Newton-Raphson procedure to solve the nonlinear system (14) we obtain at every Newton step a matrix system of the form

$$\begin{bmatrix} A & B & E \\ C & D & L \\ M & N & P \end{bmatrix} \begin{pmatrix} Q \\ U \\ \Lambda \end{pmatrix} = \begin{pmatrix} H \\ F \\ G \end{pmatrix},$$

where $Q$, $U$ and $\Lambda$ are the vectors of degrees of freedom of $\boldsymbol{q}_h$, $\boldsymbol{u}_h$ and $\widehat{\boldsymbol{u}}_h$, respectively. We note that the degrees of freedom for $\boldsymbol{q}_h$, $\boldsymbol{u}_h$ are grouped together and ordered in an element-wise fashion, the corresponding matrix $[A\ B; C\ D]$ has block-diagonal structure. The size of each block is given by the number of degrees of freedom of $\boldsymbol{q}_h$, $\boldsymbol{u}_h$ associated to each element. Therefore, we can eliminate both $\boldsymbol{Q}$ and $U$ to obtain a reduced system in terms of $\Lambda$ as

$$\mathbb{A}\,\Lambda = \mathbb{F},$$

where

$$\mathbb{A} = P - \begin{bmatrix} M & N \end{bmatrix} \begin{bmatrix} A & B \\ C & D \end{bmatrix}^{-1} \begin{bmatrix} E \\ L \end{bmatrix}, \qquad \mathbb{F} = G - \begin{bmatrix} M & N \end{bmatrix} \begin{bmatrix} A & B \\ C & D \end{bmatrix}^{-1} \begin{bmatrix} H \\ F \end{bmatrix}.$$

The matrix $\mathbb{A}$ has the same size and structure as the matrix $\mathbb{K}$ of the HDG method for the Euler equations.

## C. Stabilization Matrix

We add to the stabilization matrix of the HDG method for the Euler equations a viscous component $\boldsymbol{S}_{\text{diff}}$. In particular, for the first scheme (5), the stabilization matrix becomes

$$\boldsymbol{S} = \boldsymbol{L}|\boldsymbol{\Lambda}|\boldsymbol{R} + \boldsymbol{S}_{\text{diff}}, \tag{16}$$

whereas for the second scheme (6), it is given by

$$\boldsymbol{S} = \lambda_{\max}\boldsymbol{I} + \boldsymbol{S}_{\text{diff}}. \tag{17}$$

The matrix $\boldsymbol{S}_{\text{diff}}$ is taken to be diagonal and given by the coefficients of the diffusive terms in the momentum and energy equations. If we non-dimensionalize the Navier-Stokes equations with respect to a reference length, velocity, density and temperature, the non-dimensional viscosity coefficient in the momentum equation becomes $k_m = 1/Re$, and the temperature diffusion coefficient in the energy equation becomes $k_e = 1/((\gamma - 1)M_\infty^2 RePr)$. Here, $M_\infty$ is the Mach number defined by the reference conditions, $Re$ is the Reynolds number, $Pr$ is the Prandtl number and $\gamma$ is the adiabatic index. Therefore, we choose

$$\boldsymbol{S}_{\text{diff}} = \begin{pmatrix} 0 & & & \\ & k_m & & \\ & & k_m & \\ & & & k_e \end{pmatrix}. \tag{18}$$

For compressible viscous flows, the Reynolds number is typically very large and hence the contribution of $\boldsymbol{S}_{\text{diff}}$ is very small. However, in some cases where the Reynolds number is small, the viscous component plays an important role in the accuracy of the method. We have also experienced and obtained similar results with a diffusion stabilization matrix of the form $\boldsymbol{S}_{\text{diff}} = \alpha I$, where $\alpha$ is a scalar of the order of $1/Re$ and $I$ is the identity matrix.

American Institute of Aeronautics and Astronautics

## D.   Wall Boundary Conditions

At the solid surface with no slip, we impose zero velocity and either a fixed temperature $T = T_w$ (isothermal wall) or zero heat flux $\partial T/\partial \boldsymbol{n} = 0$ (adiabatic wall). First, we note that the first component of both $\boldsymbol{F}(\boldsymbol{u}) \cdot \boldsymbol{n}$ and $\boldsymbol{G}(\boldsymbol{u}, \boldsymbol{q}) \cdot \boldsymbol{n}$ vanishes at the solid wall since $\boldsymbol{u}$ is zero there. Therefore, we must set the first component of $\widehat{\boldsymbol{B}}_h$ equal to the first component of $\widehat{\boldsymbol{F}}_h + \widehat{\boldsymbol{G}}_h$ which will be set to zero weakly. We then set the next $m - 2$ (velocity) components of $\widehat{\boldsymbol{B}}_h$ to be equal to the velocity components of $\widehat{\boldsymbol{u}}_h$, which in turn weakly enforces the velocity components of $\widehat{\boldsymbol{u}}_h$ to be zero at the wall. The last component of $\widehat{\boldsymbol{B}}_h$ depends on wether the wall is isothermal or adiabatic. For the adiabatic wall, we set the last component of $\widehat{\boldsymbol{B}}_h$ equal to the last component of $\widehat{\boldsymbol{F}}_h + \widehat{\boldsymbol{G}}_h$ since the last component of both $\boldsymbol{F}(\boldsymbol{u}) \cdot \boldsymbol{n}$ and $\boldsymbol{G}(\boldsymbol{u}, \boldsymbol{q}) \cdot \boldsymbol{n}$ vanishes at the solid wall. For the isothermal wall, we set the last component of $\widehat{\boldsymbol{B}}_h$ to $T_w - \widehat{T}_h$, where $\widehat{T}_h$ is the approximate trace of the temperature and determined from $\widehat{\boldsymbol{u}}_h$.

## E.   Extension to the Unsteady Navier-Stokes Equations

Finally, we extend the HDG method to the unsteady Navier-Stokes equations

$$
\begin{aligned}
\boldsymbol{q} - \nabla \boldsymbol{u} &= 0, & \text{in } \Omega \times (0, t_f], \\
\frac{\partial \boldsymbol{u}}{\partial t} + \nabla \cdot (\boldsymbol{F}(\boldsymbol{u}) + \boldsymbol{G}(\boldsymbol{u}, \boldsymbol{q})) &= 0, & \text{in } \Omega \times (0, t_f], \\
\boldsymbol{u} &= \boldsymbol{u}_0, & \text{on } \Omega \times \{t = 0\}.
\end{aligned}
$$

The boundary conditions are the same as the steady-state case.

For simplicity of exposition we use the Backward-Euler scheme to discretize the time derivative with timestep $\Delta t^j$ for $j \geq 1$. At time level $t^j$ we seek an approximation $(\boldsymbol{q}_h^j, \boldsymbol{u}_h^j, \widehat{\boldsymbol{u}}_h^j) \in \boldsymbol{V}_h^k \times \boldsymbol{W}_h^k \times \boldsymbol{M}_h^k$ such that

$$
\begin{aligned}
\left(\boldsymbol{q}_h^j, \boldsymbol{v}\right)_{\mathcal{T}_h} + (\boldsymbol{u}_h^j, \nabla \cdot \boldsymbol{v})_{\mathcal{T}_h} - \left\langle \widehat{\boldsymbol{u}}_h^j, \boldsymbol{v} \cdot \boldsymbol{n} \right\rangle_{\partial \mathcal{T}_h} &= 0, & \forall \boldsymbol{w} \in \boldsymbol{V}_h^k, \\
\left(\frac{\boldsymbol{u}_h^j}{\Delta t}, \boldsymbol{w}\right) - \left(\boldsymbol{F}(\boldsymbol{u}_h^j) + \boldsymbol{G}(\boldsymbol{u}_h^j, \boldsymbol{q}_h^j), \nabla \boldsymbol{w}\right)_{\mathcal{T}_h} + \left\langle (\widehat{\boldsymbol{F}}_h^j + \widehat{\boldsymbol{G}}_h^j) \cdot \boldsymbol{n}, \boldsymbol{w} \right\rangle_{\partial \mathcal{T}_h} &= \left(\frac{\boldsymbol{u}_h^{j-1}}{\Delta t}, \boldsymbol{w}\right), & \forall \boldsymbol{w} \in \boldsymbol{W}_h^k, \\
\left\langle (\widehat{\boldsymbol{F}}_h^j + \widehat{\boldsymbol{G}}_h^j) \cdot \boldsymbol{n}, \boldsymbol{\mu} \right\rangle_{\partial \mathcal{T}_h \setminus \partial \Omega} + \left\langle \widehat{\boldsymbol{B}}_h^j, \boldsymbol{\mu} \right\rangle_{\partial \Omega} &= 0, & \forall \boldsymbol{\mu} \in \boldsymbol{M}_h^k.
\end{aligned}
$$
$$\tag{19}$$

As before, we define the interior numerical fluxes as

$$
(\widehat{\boldsymbol{F}}_h^j + \widehat{\boldsymbol{G}}_h^j) \cdot \boldsymbol{n} = (\boldsymbol{F}(\widehat{\boldsymbol{u}}_h^j) + \boldsymbol{G}(\widehat{\boldsymbol{u}}_h^j, \boldsymbol{q}_h^j)) \cdot \boldsymbol{n} + \boldsymbol{S}(\boldsymbol{u}_h^j, \widehat{\boldsymbol{u}}_h^j)(\boldsymbol{u}_h^j - \widehat{\boldsymbol{u}}_h^j),
\tag{20}
$$

and the boundary numerical flux $\widehat{\boldsymbol{B}}_h^j$ as already described in the previous subsection. Since this discrete nonlinear system is similar to the system (14) for the steady-state case, we apply the same solution procedure described above for the steady-state case to the time-dependent case at every time level.

# IV.   Numerical Results

We present in this section three representative examples to assess the accuracy and convergence of the proposed method. The first example is a compressible inviscid flow over a Kármán-Trefftz airfoil, by which we compare the computed solution with an exact incompressible potential solution. The second example is the compressible Couette flow with a source term, by which we examine the convergence of the method. The last example is a compressible laminar flow over the same Kármán-Trefftz airfoil, by which we illustrate the benefit of using high-order approximations.

## A.   Euler flow

The first example we consider is that of an inviscid flow over an airfoil. The geometry of the airfoil is obtained by transforming a circle in the complex $\zeta$-plane into the complex $z$-plane using a Kármán-Trefftz trasnformation

$$
\frac{z - n}{z + n} = \left(\frac{\zeta - 1}{\zeta + 1}\right)^n
\tag{21}
$$

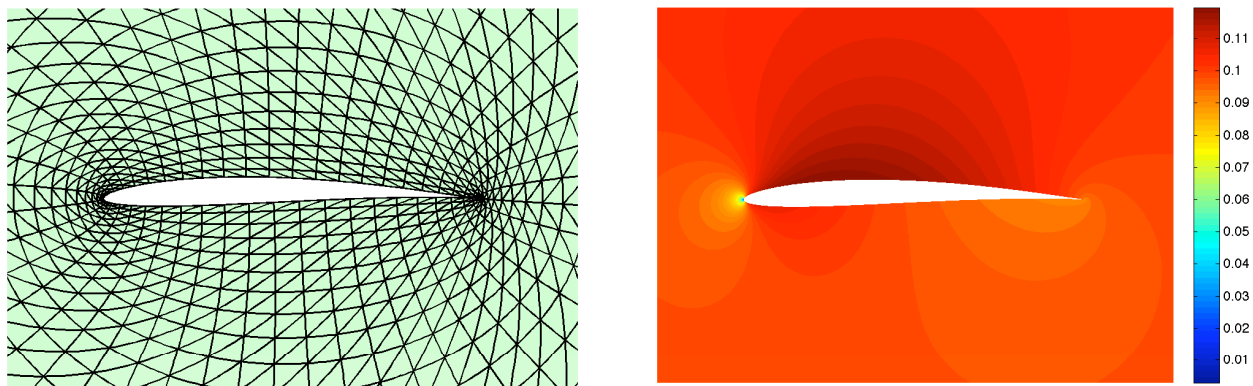American Institute of Aeronautics and Astronautics

**Figure 1. Inviscid flow over a Kármán-Trefftz airfoil: $M_\infty = 0.1$, $\alpha = 0$. Detail of the mesh employed (left) and Mach number contours of the solution using fourth order polynomial approximations (right).**
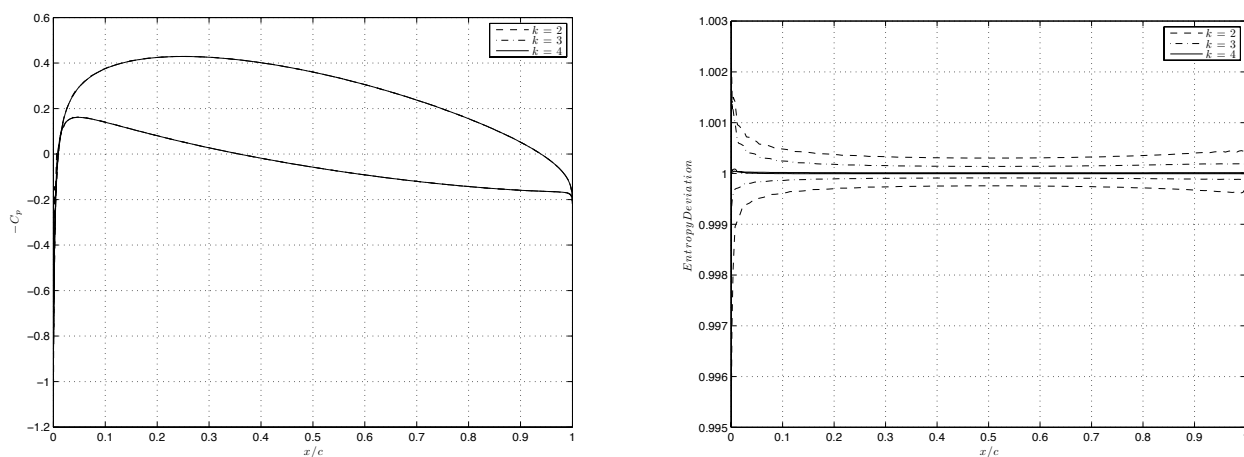


**Figure 2. Inviscid flow over a Kármán-Trefftz airfoil: $M_\infty = 0.1$, $\alpha = 0$. Pressure coefficient distribution (left) and entropy deviation (right) over the airfoil surface.**

For the particular airfoil considered here the circle on the $\zeta$-plane is centered at point $(-0.05, 0.05)$ and the radius of the circle is such that it passes through the point $(1, 0)$. The value of $n$ determines the trailing edge angle $\beta_t$, and for our example it is chosen as $n = 2 - \beta_t/\pi = 1.98$. The results reported below have been done with the stabilization matrix given by equation (5), but we have found no appreciable differences when using the alternative simpler stabilization form given by equation (6).

The airfoil geometry as well as a detail of the mesh utilized in all our computations is shown in figure 1. We have dealt with the curved elements by mapping them into a master element with uniform node spacing using an isoparametric mapping. The figure also shows the Mach number contours obtained for a free stream Mach number $M_\infty = 0.1$ and an angle of attach $\alpha = 0$ using fourth order polynomial approximations ($k = 4$). The distribution of pressure coefficient and entropy deviation $s = (p/p_\infty)/(\rho/\rho_\infty)^\gamma$ over the airfoil surface is shown in figure 2 for polynomial approximations $k = 2, 3$ and $4$. While there is no appreciable difference in the pressure coefficient, the entropy deviation is reduced considerably every time the order of approximation is increased.

In order to validate this solution, we show in figure 3 the comparison of the pressure coefficient calculated with $k = 4$ and the analytical potential solution for the incompressible case. The very minor differences between the two solutions can be attributed to compressibility effects as well as to the proximity of the far field boundary in the Euler computations. In the computations, the far field boundary has only been placed at a distance of five chords away from the airfoil and no vortex correction has been applied. Note that even in this case, the errors are expected to be small since the angle of attack considered is zero and hence the lift is small which in turn implies that the first order vortex correction would also be small.
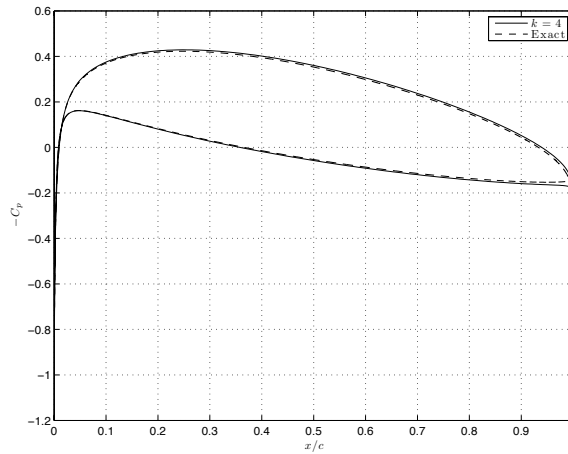
American Institute of Aeronautics and Astronautics

**Figure 3. Inviscid flow over a Kármán-Trefftz airfoil at** $\alpha = 0$. **Comparison of the pressure coefficient between the HDG solution for** $M_\infty = 0.1$ **using a** $k = 4$ **approximation and the exact incompressible potential solution.**

## B. Couette Flow

This example is aimed at verifying the accuracy and convergence of the method for the Navier-Stokes equations. We consider a compressible Couette flow with a source term on a square domain ($0 \leq x \leq H$ and $0 \leq y \leq H$). The exact solution is given by

$$u = U\overline{y}\log\left(1 + \overline{y}\right), \quad v = 0, \quad p = p_\infty \quad \text{and} \quad T = T_0 + \overline{y}(T_1 - T_0) + \frac{\gamma - 1}{2\gamma p_\infty}Pr\overline{y}\left(1 - \overline{y}\right),$$

where $\overline{y} = y/H$. The density is is then given by $\rho = 1/T$. The source term is determined from the exact solution as

$$\boldsymbol{s} = \left(0, \; -\frac{\overline{y} + 2}{(\overline{y} + 1)^2}, \; 0, \; \frac{3\log(\overline{y} + 1) + \overline{y}(2\log(\overline{y} + 1) + 2) + 1}{(\overline{y} + 1)^2} - 3\log(\overline{y} + 1) - \log(\overline{y} + 1)^2\right).$$

For our numerical experiments we take $U = 1$, $H = 1$, $T_0 = 0.8$ and $T_1 = 0.85$, $Pr = 0.72$ and $p_\infty = 1/(\gamma M_\infty^2)$ with $M_\infty = 0.15$. Even though the velocity, pressure and temperature distribution are independent of the Reynolds number, $Re$, we are interested in evaluating the stresses which are a function of $Re$. For this problem we set the unit Reynolds number to unity. The computational domain is discretized into a uniform square mesh and then each square is further divided into two triangles.

In order to asses the accuracy of the computed solution we calculate the $L^2$-norm of the error in the density $\rho$, the linear momentum vector $\boldsymbol{p} = (\rho u, \rho v)$, the energy $\rho E$, the heat flux $\boldsymbol{h} = \nabla T$, and the stress tensor

$$\boldsymbol{\tau} = \left(\begin{array}{cc} \frac{2}{3}(2u_x - v_y) + p & u_y + v_x \\ u_y + v_x & \frac{2}{3}(2v_y - u_x) + p \end{array}\right)$$

for different mesh sizes and different polynomial orders. We display the computed errors and orders of convergence for the approximations to these quantities in Table 1 for the choice of the stabilization matrix (16) and in Table 2 for the choice of the stabilization matrix (17). Note here that the approximate stresses $\boldsymbol{\tau}_h$ and heat flux $\boldsymbol{h}_h$ are computed based on the approximate conserved variables $\boldsymbol{u}_h$ and the approximate gradients $\boldsymbol{q}_h$. We observe that the $L^2$-norm of the error in these approximate quantities converges with the optimal order of accuracy of $k + 1$.

## C. Navier-Stokes flow

The final example we consider is a laminar flow over an airfoil. The geometry of the airfoil and the mesh employed is the same that has been used for the Euler example. The characteristics of the flow are $M_\infty = 0.1$, $Re = 4,000$ and $Pr = 0.72$. Since the Reynolds number is large, the viscous component (the second term) in

American Institute of Aeronautics and Astronautics

| degree $k$ | mesh $1/h$ | $\|\rho - \rho_h\|_{\mathcal{T}_h}$ error | order | $\|\boldsymbol{p} - \boldsymbol{p}_h\|_{\mathcal{T}_h}$ error | order | $\|\rho E - \rho E_h\|_{\mathcal{T}_h}$ error | order | $\|\boldsymbol{\tau} - \boldsymbol{\tau}_h\|_{\mathcal{T}_h}$ error | order | $\|\boldsymbol{h} - \boldsymbol{h}_h\|_{\mathcal{T}_h}$ error | order |
|---|---|---|---|---|---|---|---|---|---|---|---|
| 1 | 2 | 9.50e-4 | –– | 1.21e-2 | –– | 1.65e-2 | –– | 3.59e-2 | –– | 4.87e-3 | –– |
|   | 4 | 1.56e-4 | 2.60 | 3.15e-3 | 1.95 | 4.32e-3 | 1.93 | 1.07e-2 | 1.74 | 1.3e-3 | 1.91 |
|   | 8 | 2.62e-5 | 2.58 | 8.05e-4 | 1.97 | 9.66e-4 | 2.16 | 2.96e-3 | 1.86 | 2.95e-4 | 2.14 |
|   | 16 | 4.71e-6 | 2.48 | 2.04e-4 | 1.98 | 2.06e-4 | 2.23 | 7.95e-4 | 1.89 | 6.16e-5 | 2.26 |
|   | 32 | 9.55e-7 | 2.30 | 5.13e-5 | 1.99 | 4.56e-5 | 2.17 | 2.13e-4 | 1.90 | 1.30e-5 | 2.25 |
|   | 64 | 2.21e-7 | 2.11 | 1.29e-5 | 1.99 | 1.09e-5 | 2.06 | 5.72e-5 | 1.89 | 2.91e-6 | 2.16 |
| 2 | 2 | 4.69e-5 | –– | 6.84e-4 | –– | 1.97e-3 | –– | 2.60e-3 | –– | 2.77e-4 | –– |
|   | 4 | 6.59e-6 | 2.83 | 9.22e-5 | 2.89 | 3.55e-4 | 2.47 | 4.44e-4 | 2.55 | 3.50e-5 | 2.98 |
|   | 8 | 9.79e-7 | 2.75 | 1.18e-5 | 2.97 | 5.92e-5 | 2.58 | 7.05e-5 | 2.66 | 3.92e-6 | 3.16 |
|   | 16 | 1.60e-7 | 2.62 | 1.49e-6 | 2.99 | 1.01e-5 | 2.55 | 1.10e-5 | 2.69 | 4.10e-7 | 3.26 |
|   | 32 | 2.69e-8 | 2.57 | 1.88e-7 | 2.99 | 1.72e-6 | 2.55 | 1.70e-6 | 2.69 | 4.36e-8 | 3.23 |
|   | 64 | 4.45e-9 | 2.60 | 2.37e-8 | 2.99 | 2.85e-7 | 2.59 | 2.61e-7 | 2.70 | 4.93e-9 | 3.14 |
| 3 | 2 | 4.06e-6 | –– | 4.61e-5 | –– | 1.40e-4 | –– | 2.10e-4 | –– | 2.66e-5 | –– |
|   | 4 | 2.68e-7 | 3.92 | 3.30e-6 | 3.81 | 1.21e-5 | 3.53 | 1.95e-5 | 3.43 | 2.51e-6 | 3.41 |
|   | 8 | 1.60e-8 | 4.06 | 2.11e-7 | 3.97 | 8.92e-7 | 3.76 | 1.59e-6 | 3.61 | 1.68e-7 | 3.90 |
|   | 16 | 9.98e-10 | 4.01 | 1.30e-8 | 4.02 | 6.16e-8 | 3.86 | 1.21e-7 | 3.72 | 9.02e-9 | 4.22 |
|   | 32 | 6.42e-11 | 3.96 | 8.03e-10 | 4.02 | 4.09e-9 | 3.91 | 8.74e-9 | 3.79 | 4.22e-10 | 4.42 |
|   | 64 | 4.12e-12 | 3.96 | 4.96e-11 | 4.02 | 2.64e-10 | 3.95 | 6.01e-10 | 3.86 | 1.92e-11 | 4.46 |
| 4 | 2 | 3.45e-7 | –– | 3.50e-6 | –– | 1.53e-5 | –– | 1.99e-5 | –– | 2.36e-6 | –– |
|   | 4 | 1.66e-8 | 4.38 | 1.33e-7 | 4.71 | 9.43e-7 | 4.02 | 1.08e-6 | 4.20 | 9.4e-8 | 4.65 |
|   | 8 | 7.51e-10 | 4.46 | 4.33e-9 | 4.94 | 4.67e-8 | 4.34 | 4.82e-8 | 4.49 | 2.6e-9 | 5.17 |
|   | 16 | 3.07e-11 | 4.61 | 1.35e-10 | 5.01 | 1.95e-9 | 4.58 | 1.88e-9 | 4.68 | 6.64e-11 | 5.29 |
|   | 32 | 1.15e-12 | 4.74 | 4.16e-12 | 5.01 | 7.35e-11 | 4.73 | 6.75e-11 | 4.80 | 1.87e-12 | 5.15 |

**Table 1. History of convergence of the HDG method for the compressible Couette flow with a source term. The results are obtained by using the stabilization matrix (16).**

(16) is relatively small. As a consequence, we have found no appreciable differences in the numerical results whether using the stabilization form (16) or (5).

Figure 4 shows the Mach contours of the solution computed using a fourth order polynomial approximation. Also shown in the figure is a detail of the mesh and solution near the leading edge. where one can observed that a high order element is actually sufficient to cleanly capture the boundary layer. In order to verify that this is a grid converged solution we show in Figure 5 the distribution of pressure and skin friction coefficient using polynomial approximations of $k = 2, 3$ and $4$. It can be readily observed that differences in the surface quantities computed for the different orders of approximation are very small.

## V.   Conclusions

We have presented a hybridizable discontinuous Galerkin method for the numerical solution of the compressible Euler and Navier-Stokes equations. The proposed method holds important advantages over many existing DG methods in terms of the globally coupled degrees of freedom and in the improved accuracy. Moreover, the HDG method is somewhat simpler to implement than other implicit DG methods and allows for the simple treatment of boundary conditions and numerical fluxes. The numerical results show that the HDG method is efficient for the numerical simulation of inviscid and viscous compressible flows. Our current research is focused on the development of efficient iterative methods for solving the linear system which arises from application of the Newton-Raphson procedure.

## Acknowledgments

| degree $k$ | mesh $1/h$ | $\|\rho - \rho_h\|_{\mathcal{T}_h}$ error | order | $\|\boldsymbol{p} - \boldsymbol{p}_h\|_{\mathcal{T}_h}$ error | order | $\|\rho E - \rho E_h\|_{\mathcal{T}_h}$ error | order | $\|\boldsymbol{\tau} - \boldsymbol{\tau}_h\|_{\mathcal{T}_h}$ error | order | $\|\boldsymbol{h} - \boldsymbol{h}_h\|_{\mathcal{T}_h}$ error | order |
|---|---|---|---|---|---|---|---|---|---|---|---|
| 1 | 2 | 5.10e-4 | –– | 1.20e-2 | –– | 1.71e-2 | –– | 7.46e-2 | –– | 2.25e-3 | –– |
|  | 4 | 1.08e-4 | 2.24 | 2.83e-3 | 2.08 | 5.97e-3 | 1.51 | 2.42e-2 | 1.63 | 5.60e-4 | 2.00 |
|  | 8 | 2.34e-5 | 2.2 | 6.89e-4 | 2.04 | 1.42e-3 | 2.07 | 6.92e-3 | 1.80 | 1.80e-4 | 1.64 |
|  | 16 | 4.98e-6 | 2.23 | 1.70e-4 | 2.02 | 3.06e-4 | 2.21 | 1.86e-3 | 1.90 | 6.16e-5 | 1.55 |
|  | 32 | 1.04e-6 | 2.26 | 4.24e-5 | 2.01 | 6.45e-5 | 2.25 | 4.81e-4 | 1.95 | 1.98e-5 | 1.64 |
|  | 64 | 2.20e-7 | 2.25 | 1.06e-5 | 2.00 | 1.37e-5 | 2.23 | 1.23e-4 | 1.97 | 5.83e-6 | 1.76 |
| 2 | 2 | 2.92e-5 | –– | 6.32e-4 | –– | 1.9e-3 | –– | 4.75e-3 | –– | 2.39e-4 | –– |
|  | 4 | 4.41e-6 | 2.73 | 7.99e-5 | 2.98 | 2.96e-4 | 2.69 | 7.46e-4 | 2.67 | 4.33e-5 | 2.46 |
|  | 8 | 6.09e-7 | 2.86 | 9.94e-6 | 3.01 | 4.07e-5 | 2.86 | 1.05e-4 | 2.83 | 7.51e-6 | 2.53 |
|  | 16 | 8.20e-8 | 2.89 | 1.24e-6 | 3.01 | 5.45e-6 | 2.90 | 1.41e-5 | 2.90 | 1.22e-6 | 2.62 |
|  | 32 | 1.15e-8 | 2.84 | 1.54e-7 | 3.00 | 7.54e-7 | 2.85 | 1.85e-6 | 2.93 | 1.85e-7 | 2.73 |
|  | 64 | 1.70e-9 | 2.75 | 1.93e-8 | 3.00 | 1.11e-7 | 2.77 | 2.42e-7 | 2.94 | 2.60e-8 | 2.83 |
| 3 | 2 | 2.92e-6 | –– | 3.94e-5 | –– | 1.78e-4 | –– | 3.45e-4 | –– | 1.32e-5 | –– |
|  | 4 | 2.41e-7 | 3.60 | 2.70e-6 | 3.86 | 1.52e-5 | 3.55 | 2.81e-5 | 3.62 | 1.39e-6 | 3.24 |
|  | 8 | 1.69e-8 | 3.83 | 1.73e-7 | 3.96 | 1.08e-6 | 3.82 | 2.01e-6 | 3.80 | 1.23e-7 | 3.50 |
|  | 16 | 1.13e-9 | 3.91 | 1.09e-8 | 4.00 | 7.25e-8 | 3.90 | 1.38e-7 | 3.87 | 9.71e-9 | 3.66 |
|  | 32 | 7.51e-11 | 3.91 | 6.77e-10 | 4.00 | 4.83e-9 | 3.91 | 9.38e-9 | 3.88 | 7.05e-10 | 3.78 |
|  | 64 | 4.97e-12 | 3.92 | 4.22e-11 | 4.01 | 3.19e-10 | 3.92 | 6.35e-10 | 3.88 | 4.79e-11 | 3.88 |
| 4 | 2 | 2.99e-7 | –– | 2.83e-6 | –– | 1.86e-5 | –– | 2.79e-5 | –– | 1.63e-6 | –– |
|  | 4 | 1.43e-8 | 4.39 | 1.05e-7 | 4.74 | 9.05e-7 | 4.36 | 1.24e-6 | 4.49 | 9.36e-8 | 4.12 |
|  | 8 | 6.01e-10 | 4.57 | 3.48e-9 | 4.92 | 3.83e-8 | 4.56 | 4.79e-8 | 4.69 | 4.24e-9 | 4.46 |
|  | 16 | 2.43e-11 | 4.63 | 1.10e-10 | 4.98 | 1.56e-9 | 4.62 | 1.77e-9 | 4.76 | 1.68e-10 | 4.66 |
|  | 32 | 9.48e-13 | 4.68 | 3.43e-12 | 5.00 | 6.07e-11 | 4.68 | 6.36e-11 | 4.80 | 6.10e-12 | 4.78 |

**Table 2. History of convergence of the HDG method for the compressible Couette flow with a source term. The results are obtained by using the stabilization matrix (17).**

# References

[1] D. A. Anderson, J. C. Tannehill, and R. H. Pletcher. *Computational Fluid Dynamics and Heat Transfer*. Hemisphere Publishing, New York, 1984.

[2] D. N. Arnold, F. Brezzi, B. Cockburn, and L. D. Marini. Unified analysis of discontinuous Galerkin methods for elliptic problems. *SIAM J. Numer. Anal.*, 39(5):1749–1779, 2001.

[3] F. Bassi and S. Rebay. A high-order accurate discontinuous finite element method for the numerical solution of the compressible Navier-Stokes equations. *J. Comput. Phys.*, 131:267–279, 1997.

[4] C. Baumann and J. Oden. A discontinuous hp finite element method for convection-diffusion problems. *Comput. Methods Appl. Mech. Engrg.*, 175:311–341, 1999.

[5] B. Cockburn. Discontinuous Galerkin methods. *ZAMM Z. Angew. Math. Mech.*, 83:731–754, 2003.

[6] B. Cockburn. Discontinuous Galerkin Methods for Computational Fluid Dynamics. In R. de Borst E. Stein and T.J.R. Hughes, editors, *Encyclopedia of Computational Mechanics*, volume 3, pages 91–123. John Wiley & Sons, Ltd., England, 2004.

[7] B. Cockburn, J. Gopalakrishnan, and R. Lazarov. Unified hybridization of discontinuous Galerkin, mixed and continuous Galerkin methods for second order elliptic problems. *SIAM J. Numer. Anal.*, 47:1319–1365, 2009.

[8] B. Cockburn, B. Dong, J. Guzman, M. Restelli, and R. Sacco. A Hybridizable Discontinuous Galerkin Method for Steady-State Convection-Diffusion-Reaction Problems *SIAM J. Sci. Comput.* 31:3827, 2009.

[9] B. Cockburn, J. Gopalakrishnan, N. C. Nguyen, J. Peraire, and F-J Sayas. Analysis of an HDG method for Stokes flow. *Math. Comp.*. To appear.

[10] B. Cockburn and C. W. Shu. The local discontinuous Galerkin method for convection-diffusion systems. *SIAM J. Numer. Anal.*, 35:2440–2463, 1998.

[11] B. Cockburn and C.-W. Shu. Runge-Kutta discontinuous Galerkin methods for convection-dominated problems. *J. Sci. Comput.*, 16:173–261, 2001.

[12] I. Lomtev and G. E. Karniadakis. A discontinuous Galerkin method for the Navier-Stokes equations. *International Journal for Numerical Methods in Fluids*, 29:587–603, 1999.

[13] N. C. Nguyen, J. Peraire, and B. Cockburn. An implicit high-order hybridizable discontinuous Galerkin method for linear convection-diffusion equations. *J. Comput. Phys.*, 228:3232–3254, 2009.
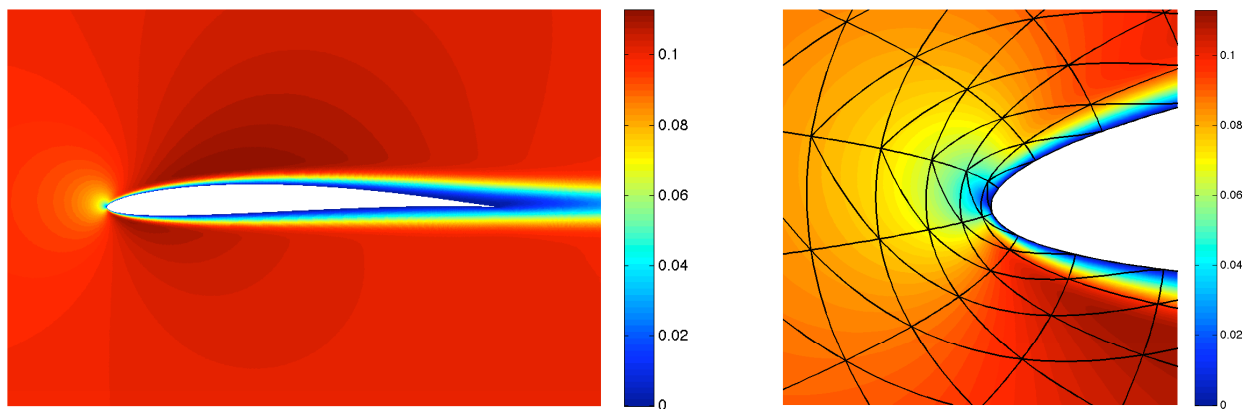
**Figure 4. Inviscid flow over a Kármán-Trefftz airfoil:** $M_\infty = 0.1$, $Re = 4000$ **and** $\alpha = 0$. **Mach number distribution (left) and detail of the mesh and Mach number solution near the leading edge region (right) using fourth order polynomial approximations.**
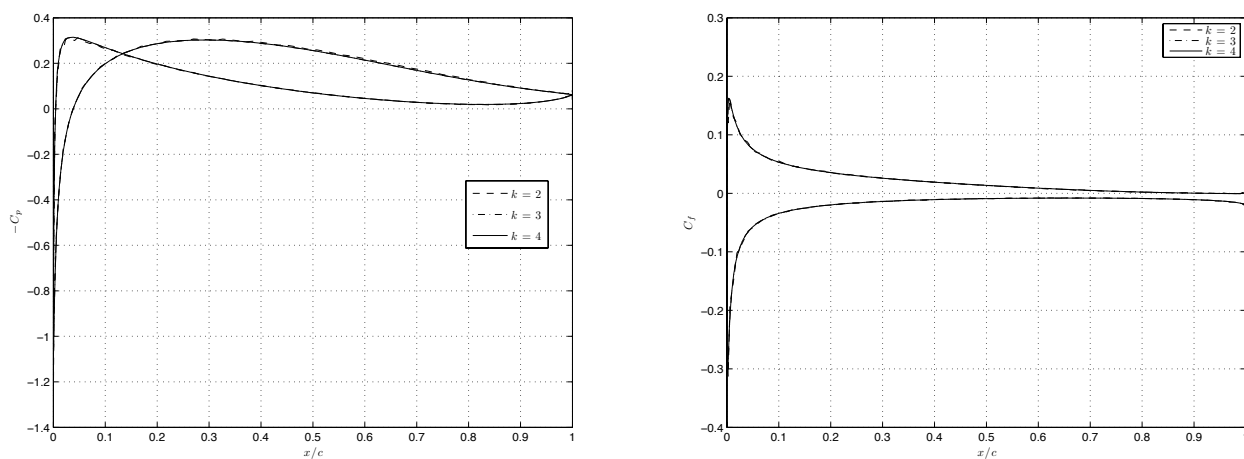


**Figure 5. Laminar flow over a Kármán-Trefftz airfoil:** $M_\infty = 0.1$, $Re = 4000$ **and** $\alpha = 0$. **Pressure coefficient distribution (left) and skin friction coefficient (right) over the airfoil surface.**

[14]N. C. Nguyen, J. Peraire, and B. Cockburn. An implicit high-order hybridizable discontinuous Galerkin method for nonlinear convection-diffusion equations. *J. Comput. Phys.*, 228:8841–8855, 2009.

[15]N.C. Nguyen, J. Peraire, and B. Cockburn, A hybridizable discontinuous Galerkin method for Stokes flow. *Computer Methods in Applied Mechanics and Engineering*. To appear.

[16]N.C. Nguyen, J. Peraire, and B. Cockburn, A comparison of HDG methods for Stokes flow. Submitted.

[17]N.C. Nguyen, J. Peraire, and B. Cockburn, A hybridizable discontinuous Galerkin method for the incompressible Navier-Stokes equations. Submitted.

[18]N.C. Nguyen, P.O. Persson, and J. Peraire, RANS Solutions using high order discontinuous Galerkin methods. In Proceedings of the 45th AIAA Aerospace Sciences Meeting and Exhibit, AIAA-2007-0914, Reno, NV, January 2007.

[19]J. Peraire and P. O. Persson. The compact discontinuous Galerkin (CDG) method for elliptic problems. *SIAM Journal on Scientific Computing*, 30(4):1806–1824, 2008.

[20]P. O. Persson and J. Peraire. Newton-GMRES preconditioning for discontinuous Galerkin discretizations of the Navier-Stokes equations. *SIAM Journal on Scientific Computing*, 30(6):2709–2733, 2008.

[21]R. Hartmann and P. Houston An optimal order interior penalty discontinuous Galerkin discretization of the compressible Navier-Stokes equations. *J. Comput. Phys.*, 227:9670–9685, 2008.

[22]W.H. Reed and T.R. Hill. Triangular mesh methods for the neutron transport equation. Technical Report LA-UR-73-479, Los Alamos Scientific Laboratory, 1973.